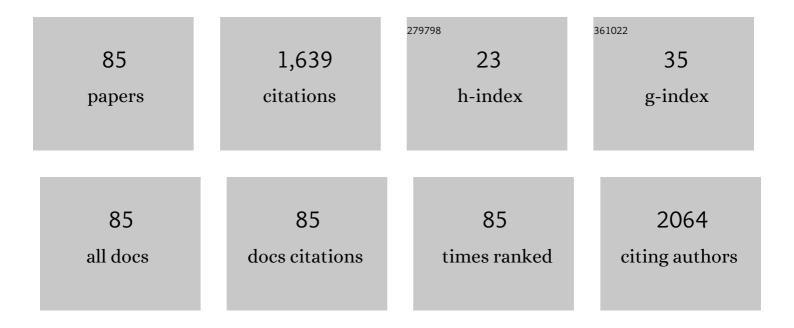
List of Publications by Year in descending order

Source: https://exaly.com/author-pdf/6617207/publications.pdf Version: 2024-02-01



ΙΔΝΕΖ ΖΑΝΑΔ:ΝΙΚ

#	Article	IF	CITATIONS
1	On the mechanism of visible-light accelerated methane dry reforming reaction over Ni/CeO2â^'x catalysts. Applied Catalysis B: Environmental, 2022, 301, 120745.	20.2	40
2	Degradation of asbestos – Reinforced water supply cement pipes after a long-term operation. Chemosphere, 2022, 287, 131977.	8.2	4
3	Advancing Li-ion storage performance with hybrid vertical carbon/Ni3S2-based electrodes. Journal of Energy Chemistry, 2022, 67, 8-18.	12.9	17
4	N-Graphene-Metal-Oxide(Sulfide) hybrid Nanostructures: Single-step plasma-enabled approach for energy storage applications. Chemical Engineering Journal, 2022, 430, 133153.	12.7	13
5	Effect of Au loading on Schottky barrier height in TiO2Â+ÂAu plasmonic photocatalysts. Applied Surface Science, 2022, 579, 152196.	6.1	26
6	Non-uniform He bubble formation in W/W2C composite: Experimental and ab-initio study. Acta Materialia, 2022, 226, 117608.	7.9	3
7	Evaluation of Au/ZrO2 Catalysts Prepared via Postsynthesis Methods in CO2 Hydrogenation to Methanol. Catalysts, 2022, 12, 218.	3.5	13
8	Impact of Electrolyte Incorporation in Anodized Niobium on Its Resistive Switching. Nanomaterials, 2022, 12, 813.	4.1	8
9	The influence of synthesis conditions on the visible-light triggered photocatalytic activity of g-C3N4/TiO2 composites used in AOPs. Journal of Environmental Chemical Engineering, 2022, 10, 107656.	6.7	15
10	Brookite vs. rutile vs. anatase: What`s behind their various photocatalytic activities?. Journal of Environmental Chemical Engineering, 2022, 10, 107722.	6.7	52
11	CO <sub>2</sub> Activation over Nanoshaped CeO <sub>2</sub> Decorated with Nickel for Low-Temperature Methane Dry Reforming. ACS Applied Materials & Interfaces, 2022, 14, 31862-31878.	8.0	16
12	TiO2-Î <sup>2</sup> -Bi2O3 junction as a leverage for the visible-light activity of TiO2 based catalyst used for environmental applications. Catalysis Today, 2021, 361, 165-175.	4.4	23
13	TEM investigation of pre-oxidised Fe–Al with improved aqueous corrosion resistance. Corrosion Science, 2021, 179, 109170.	6.6	10
14	Microscopic techniques for the characterisation of metal-based nanoparticles. Comprehensive Analytical Chemistry, 2021, , 241-284.	1.3	4
15	Role of CO2 During Oxidative Dehydrogenation of Propane Over Bulk and Activated-Carbon Supported Cerium and Vanadium Based Catalysts. Catalysis Letters, 2021, 151, 2816-2832.	2.6	14
16	Texture and composition of ferrian ilmenite from hornblende andesites of the Timok Magmatic Complex, Serbia. Neues Jahrbuch Fur Mineralogie, Abhandlungen, 2021, 197, 65-83.	0.3	0
17	A Novel Sensor Based on Carbon Paste Electrode Modified with Polypyrrole/Multiâ€walled Carbon Nanotubes for the Electrochemical Detection of Cytostatic Drug Rapamycin. Electroanalysis, 2021, 33, 1325-1332.	2.9	6
18	The influence of Schottky barrier height onto visible-light triggered photocatalytic activity of TiO2Â+ÂAu composites. Applied Surface Science, 2021, 543, 148799.	6.1	22

#	Article	IF	CITATIONS
19	Advanced Carbon–Nickel Sulfide Hybrid Nanostructures: Extending the Limits of Battery-Type Electrodes for Redox-Based Supercapacitor Applications. ACS Applied Materials & Interfaces, 2021, 13, 20559-20572.	8.0	39
20	Hydrogen permeability of non-stoichiometric tungsten oxides. Journal of Nuclear Materials, 2021, 548, 152860.	2.7	4
21	In-depth microscopic characterisation of the weld faying interface revealing stress-induced metallurgical transformations during friction stir spot welding. International Journal of Machine Tools and Manufacture, 2021, 164, 103716.	13.4	18
22	Dynamic recrystallization's role in strength-ductility trade-off in polycrystalline Fe–Cr–Ni stainless steels produced by laser powder bed fusion. Materials Science & Engineering A: Structural Materials: Properties, Microstructure and Processing, 2021, 814, 141214.	5.6	11
23	In situ precipitation synthesis of FeNi/ZnO nanocomposites with high microwave absorption properties. Materials Chemistry and Physics, 2021, 266, 124508.	4.0	6
24	Thickness dependent growth of Ge nanoparticles in amorphous Ge/SiO2 multilayers. Vacuum, 2021, 190, 110294.	3.5	2
25	Thermal stability studies of plasma deposited hydrogenated carbon nitride nanostructures. Carbon, 2021, 184, 82-90.	10.3	4
26	Dry reforming of methane over Ni/Ce0.8Ti0.2O2-δ: The effect of Ni particle size on the carbon pathways studied by transient and isotopic techniques. Applied Catalysis B: Environmental, 2021, 296, 120321.	20.2	62
27	Exploring the effect of morphology and surface properties of nanoshaped Pd/CeO2 catalysts on CO2 hydrogenation to methanol. Applied Catalysis A: General, 2021, 627, 118394.	4.3	22
28	Labelâ€Free Mycotoxin Raman Identification by Highâ€Performing Plasmonic Vertical Carbon Nanostructures. Small, 2021, 17, e2103677.	10.0	14
29	Defective Grey TiO2 with Minuscule Anatase–Rutile Heterophase Junctions for Hydroxyl Radicals Formation in a Visible Light-Triggered Photocatalysis. Catalysts, 2021, 11, 1500.	3.5	3
30	Evaluation of phenolic antioxidant capacity in beverages based on laccase immobilized on screen-printed carbon electrode modified with graphene nanoplatelets and gold nanoparticles. Microchemical Journal, 2020, 152, 104282.	4.5	38
31	Strength-ductility trade-off via SiC nanoparticle dispersion in A356 aluminium matrix. Materials Science & Engineering A: Structural Materials: Properties, Microstructure and Processing, 2020, 771, 138639.	5.6	19
32	Development of BMG-B2 nanocomposite structure in HAZ during laser surface processing of ZrCuNiAlTi bulk metallic glasses. Applied Surface Science, 2020, 505, 144535.	6.1	5
33	Crystal structure and composition dependence of mechanical properties of single-crystalline NbCo2 Laves phase. Acta Materialia, 2020, 184, 151-163.	7.9	29
34	Controllable voltammetric formation of a structurally disordered NiOOH/Ni(OH)2 redox pair on Ni-nanowire electrodes for enhanced electrocatalytic formaldehyde oxidation. Electrochimica Acta, 2020, 362, 137180.	5.2	24
35	Performances and Biosensing Mechanisms of Interdigitated Capacitive Sensors Based on the Hetero-mixture of SnO2 and In2O3. Sensors, 2020, 20, 6323.	3.8	2
36	Improving sensing properties of entangled carbon nanotube-based gas sensors by atmospheric plasma surface treatment. Microelectronic Engineering, 2020, 232, 111403.	2.4	14

#	Article	IF	CITATIONS
37	Electrochemical immunosensor functionalized with nanobodies for the detection of the toxic microalgae Alexandrium minutum using glassy carbon electrode modified with gold nanoparticles. Biosensors and Bioelectronics, 2020, 154, 112052.	10.1	36
38	Prospects for microwave plasma synthesized N-graphene in secondary electron emission mitigation applications. Scientific Reports, 2020, 10, 13013.	3.3	14
39	Photodegradation of Methylene Blue and Rhodamine B Using Laser-Synthesized ZnO Nanoparticles. Materials, 2020, 13, 4357.	2.9	37
40	Surface-enhanced Raman spectroscopy for chemical and biological sensing using nanoplasmonics: The relevance of interparticle spacing and surface morphology. Applied Physics Reviews, 2020, 7, .	11.3	82
41	Oriented Carbon Nanostructures from Plasma Reformed Resorcinol-Formaldehyde Polymer Gels for Gas Sensor Applications. Nanomaterials, 2020, 10, 1704.	4.1	5
42	Formation of isolated Ge nanoparticles in thin continuous Ge/SiO2 multilayers. Vacuum, 2020, 179, 109508.	3.5	3
43	Customization of Sn <sub>2</sub> P <sub>2</sub> S <sub>6</sub> ferroelectrics by post-growth solid-state diffusion doping. Journal of Materials Chemistry C, 2020, 8, 9975-9985.	5.5	4
44	Geochemistry of Bashibos-Bajrambos metasedimentary unit, Serbo-Macedonian massif, North Macedonia: Implications for age, provenance and tectonic setting. Chemie Der Erde, 2020, 80, 125664.	2.0	5
45	Reusable Au/Pd-coated chestnut-like copper oxide SERS substrates with ultra-fast self-recovery. Applied Surface Science, 2020, 517, 146205.	6.1	25
46	Deuterium transport and retention in the bulk of tungsten containing helium: the effect of helium concentration and microstructure. Nuclear Fusion, 2020, 60, 106029.	3.5	14
47	Single-Crystalline Metal Oxide Nanostructures Synthesized by Plasma-Enhanced Thermal Oxidation. Nanomaterials, 2019, 9, 1405.	4.1	26
48	TiN-Nanoparticulate-Reinforced ZrO2 for Electrical Discharge Machining. Materials, 2019, 12, 2789.	2.9	9
49	Tungsten carbide as a deoxidation agent for plasma-facing tungsten-based materials. Journal of Nuclear Materials, 2019, 524, 135-140.	2.7	12
50	Formation of a Ni(OH)2/NiOOH active redox couple on nickel nanowires for formaldehyde detection in alkaline media. Electrochimica Acta, 2019, 309, 346-353.	5.2	85
51	Electrodeposition of a Rareâ€Earth Iron Alloy from an Ionicâ€Liquid Electrolyte. ChemElectroChem, 2019, 6, 2860-2869.	3.4	31
52	New insights into nanomineralogy and geochemistry of Ni-laterite ores from central Greece (Larymna) Tj ETQqO (	0 0 rgBT /0 2.9	Dverlock 10 <sup>-</sup>
53	The role of tungsten phases formation during tungsten metal powder consolidation by FAST: Implications for high-temperature applications. Materials Characterization, 2018, 138, 308-314.	4.4	24

<sup>&</sup>lt;sup>54</sup> The role of Fe and Cu additions on the structural, thermal and magnetic properties of amorphous Al-Ce-Fe-Cu alloys. Journal of Non-Crystalline Solids, 2018, 483, 70-78.

#	Article	IF	CITATIONS
55	Modification of epoxy resin by silane-coupling agent to improve tensile properties of viscose fabric composites. Polymer Bulletin, 2018, 75, 167-195.	3.3	46
56	Stress Evolution during Ge Nanoparticles Growth in a SiO <sub>2</sub> Matrix. Inorganic Chemistry, 2018, 57, 14939-14952.	4.0	0
57	Investigation of mechanical, dynamic mechanical, rheological and morphological properties of blends based on polypropylene (PP) and cyclic olefin copolymer (COC). European Polymer Journal, 2018, 108, 439-451.	5.4	24
58	Alkali and earth alkali modified CuOx/SiO2 catalysts for propylene partial oxidation: What determines the selectivity?. Applied Catalysis B: Environmental, 2018, 237, 214-227.	20.2	32
59	Self-Ordered Voids Formation in SiO <sub>2</sub> Matrix by Ge Outdiffusion. Journal of Nanomaterials, 2018, 2018, 1-8.	2.7	4
60	Synthesis and characterization of the thermally reduced graphene oxide in argon atmosphere, and its application to construct graphene paste electrode as a naptalam electrochemical sensor. Analytica Chimica Acta, 2018, 1035, 22-31.	5.4	25
61	Paste electrode based on the thermally reduced graphene oxide in ambient air – Its characterization and analytical application for analysis of 4–chloro–3,5–dimethylphenol. Electrochimica Acta, 2018, 282, 233-241.	5.2	9
62	Mechanical, thermal, and burning properties of viscose fabric composites: Influence of epoxy resin modification. Journal of Applied Polymer Science, 2018, 135, 46673.	2.6	15
63	Electron trapping energy states of TiO 2 –WO 3 composites and their influence on photocatalytic degradation of bisphenol A. Applied Catalysis B: Environmental, 2017, 209, 273-284.	20.2	59
64	Improved electron–hole separation and migration in anatase TiO <sub>2</sub> nanorod/reduced graphene oxide composites and their influence on photocatalytic performance. Nanoscale, 2017, 9, 4578-4592.	5.6	81
65	Wiring of glucose oxidase with graphene nanoribbons: an electrochemical third generation glucose biosensor. Mikrochimica Acta, 2017, 184, 1127-1134.	5.0	57
66	Effect of samarium and vanadium co-doping on structure, ferroelectric and photocatalytic properties of bismuth titanate. RSC Advances, 2017, 7, 9680-9692.	3.6	39
67	Highly Selective Electrochemical Determination of Phlorizin Using Square Wave Voltammetry at a Boron-Doped Diamond Electrode. Food Analytical Methods, 2017, 10, 3747-3752.	2.6	16
68	Effect of the Cation Distribution and Microstructure on the Magnetic Behavior of the CoMn <sub>2</sub> O <sub>4</sub> Oxide. Inorganic Chemistry, 2017, 56, 3983-3989.	4.0	17
69	REE-bearing minerals in Drava river sediments, Slovenia, and their potential origin. Geologija, 2017, 60, 257-266.	0.4	6
70	Pyrite-pyrrhotite intergrowths in calcite marble from BistriÅįki Vintgar, Slovenia. IOP Conference Series: Materials Science and Engineering, 2016, 109, 012020.	0.6	1
71	Influence of stress on the properties of Ge nanocrystals in an SiO <sub>2</sub> matrix. Journal of Applied Crystallography, 2016, 49, 1957-1966.	4.5	6
72	Magnetoelectric studies on CoFe2O4/0.5(BaTi0.8Zr0.2O3)-0.5(Ba0.7Ca0.3TiO3) lead-free bilayer thin films derived by the chemical solution deposition. Journal of Applied Physics, 2016, 120, .	2.5	26

#	Article	IF	CITATIONS
73	Angular-dependent magnetism in Co(001) single-crystal nanowires: capturing the vortex nucleation fields. Journal of Materials Chemistry C, 2016, 4, 10664-10674.	5.5	17
74	On the origin of 'iron-cross' twins of pyrite from Mt. Katarina, Slovenia. Mineralogical Magazine, 2016, 80, 937-948.	1.4	6
75	Lowering the thermal conductivity of Sr(Ti0.8Nb0.2)O3 by SrO and CaO doping: microstructure and thermoelectric properties. Journal of Materials Science, 2016, 51, 7660-7668.	3.7	5
76	Developing high coercivity in large diameter cobalt nanowire arrays. Journal Physics D: Applied Physics, 2016, 49, 445001.	2.8	14
77	The impact of processing parameters on the properties of Zn-bonded Nd–Fe–B magnets. Journal of Magnetism and Magnetic Materials, 2016, 419, 171-175.	2.3	9
78	Determination of nitrite in tap water: A comparative study between cerium, titanium and selenium dioxide doped reduced graphene oxide modified glassy carbon electrodes. Sensors and Actuators B: Chemical, 2016, 236, 311-317.	7.8	34
79	Factors determining large observed increases in power conversion efficiency of P3HT:PCBM solar cells embedded with Mo6S9â^'xlx nanowires. Synthetic Metals, 2016, 212, 105-112.	3.9	16
80	Giant persistent photoconductivity in BaTiO3/TiO2 heterostructures. Applied Physics Letters, 2014, 105, 152101.	3.3	13
81	Sonochemical synthesis of mackinawite and the role of Cu addition on phase transformations in the Fe–S system. Journal of Nanoparticle Research, 2014, 16, 1.	1.9	12
82	Microstructures and Magnetic Properties of Electrodeposited Co-Pt Nanowires With Diameters Below 100Ânm. IEEE Magnetics Letters, 2014, 5, 1-4.	1.1	1
83	Effect of magnetocrystalline anisotropy on the magnetic properties of electrodeposited Co–Pt nanowires. Journal of Nanoparticle Research, 2014, 16, 1.	1.9	15
84	Electron microscopy study of CVT grown Fe-sulphides. Journal of Crystal Growth, 2013, 367, 18-23.	1.5	5
85	C and O stable isotopic signatures of fast-growing dripstones on alkaline substrates: reflection of growth mechanism, carbonate sources and environmental conditions. Isotopes in Environmental and Health Studies, 2012, 48, 354-371.	1.0	1